Evidence of Previous Faulting Along the 2019 Ridgecrest Earthquake Ruptures

Belle Philibosian[1], Jessica Thompson Jobe[2], Colin Chupik[2], Timothy Dawson[3], Scott Bennett[4], Ryan Gold[5], Christopher DuRoss[5], Tyler Ladinsky[3], Katherine Kendrick[6], Elizabeth Haddon[4], Ian Pierce[7], Brian Swanson[8], Gordon Seitz[3]

[1]Earthquake Science Center, U.S. Geological Survey, Moffett Field, CA; [2]Bureau of Reclamation, Denver Federal Center, Denver, CO; [3]California Geological Survey, San Mateo, CA; [4]Geology, Minerals, Energy, and Geophysics Science Center, U.S. Geological Survey, Moffett Field, CA; [5]Geologic Hazards Science Center, U.S. Geological Survey, Golden, CO; [6]Earthquake Science Center, U.S. Geological Survey, Pasadena, CA; [7]Department of Earth Sciences, University of Oxford, Oxford, UK; [8]California Geological Survey, Los Angeles, CA

Abstract

The July 2019 Ridgecrest earthquake sequence in southeastern California has been characterized as surprising because no long continuous fault lines were recognized in the area prior to these events. Only ~35% of the rupture occurred on previously mapped faults. Employing more detailed inspection of pre-event high-resolution topography and optical imagery in combination with field observations, we document evidence of active faulting in the landscape along the entire fault system. Scarps, deflected drainages, and lineaments and contrasts in topography, vegetation, and ground color demonstrate previous slip on a network of orthogonal faults, consistent with patterns of surface rupture observed in 2019 (though not all of our mapped fault strands ruptured in 2019). Outcrop-scale field observations additionally reveal tufa lineaments and sheared Quaternary deposits. Neotectonic features are commonly short (<2 km), discontinuous, and display en echelon patterns along both the M6.4 and M7.1 ruptures. These features are generally more prominent and better preserved outside the late Pleistocene lake basins. Fault expression may also be related to deformation style: scarps and topographic lineaments are more prevalent in areas where substantial vertical motion occurred in 2019. Where strike-slip displacement dominated in 2019, the faults are mainly expressed by less prominent tonal and vegetation features. Both the northeast- and northwest-trending active fault systems are subparallel to regional bedrock fabrics that were established as early as ~150 Ma, and may be reactivating these older structures. Overall, we estimate that 50–70% of the 2019 surface ruptures could have been recognized as active faults with detailed inspection of pre-event data. Similar detailed mapping of potential neotectonic features could help improve seismic hazard analyses in other regions of eastern California and elsewhere that likely have distributed faulting or incompletely mapped faults. In areas where faults cannot be resolved as single through-going structures, we recommend a zone of potential faulting should be used as a hazard model input.

The 2019 Ridgecrest earthquakes occurred on a network of NE-striking sinistral and NW-striking dextral faults in the transition zone between the ECSZ and the Walker Lane, both generally transtensional systems. Prior to the 2019 events, only about a third of the causative faults were represented in the Quaternary Fault and Fold Database (QFFD), with a handful of additional parts mapped in gray literature. However, the QFFD in this area is compiled from various sources in which mapping scale ranged from 1:750,000 to 1:24,000 and the purpose was not necessarily to identify active faults.

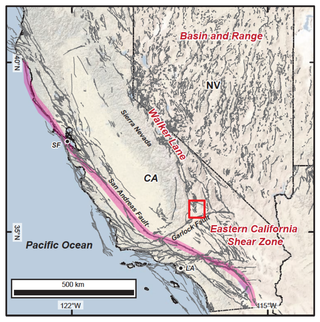

Figure 1. Tectonic setting of the study area (red box) in the ECSZ / Walker Lane in southern California. Gray lines represent active faults in the QFFD (USGS and CGS, 2019).

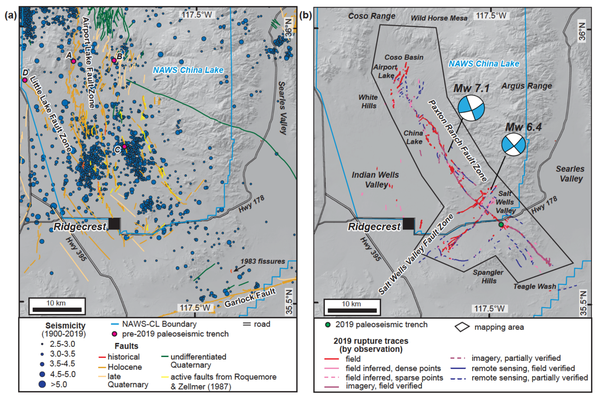

Figure 2. (a) Seismicity and previously mapped faults in the Ridgecrest area (QFFD; Roquemore and Zellmer, 1987). Seismicity displayed is from before the 2019 Ridgecrest Earthquake sequence. Location shown in Fig. 1. (b) 2019 surface rupture traces from Ponti et al. (2020). Pink dots show paleoseismic trenches from Roquemore (1981) and green dot shows 2019 paleoseismic trench from Kozaci et al. (2019). Black polygon represents mapping area of neotectonic features.

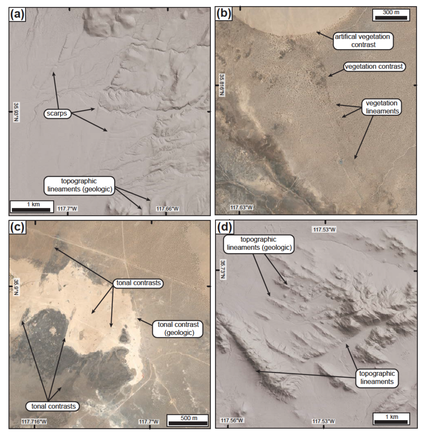

Figure 3. Examples of types of features mapped on the pre-event 2-m DEM (distributed by Willis et al., 2019 on OpenTopography.org) and imagery (Google Earth; National Agriculture Imagery Program).

It is important to recognize that in the area of the 2019 rupture, no systematic attempt at assessing fault activity using now standard-of-practice tools, such as lidar topography or large-scale high-resolution imagery, had been completed at the time of the earthquake. Using a pre-event 2-m digital elevation model (DEM), aerial and satellite imagery, and compilation of recent field observations, we mapped neotectonic features that existed in the landscape prior to the 2019 events.

We identified scarps, deflected drainages, and lineaments and contrasts in topography, vegetation, and ground color. Outcrop-scale field observations additionally reveal tufa lineaments and sheared Quaternary deposits.

Our mapping reveals evidence for previous Quaternary fault movement on a network of orthogonal faults, including most of the 2019 surface ruptures (both primary and secondary) as well as additional subparallel structures that did not move in 2019. Features are generally less promient and less numerous below the highstands of pluvial lakes, suggesting that lacustrine processes reduced preservation of neotectonic features. Scarps and other topographic features are also more common toward the ends of the Paxton Ranch FZ, where vertical deformation was more significant in 2019.

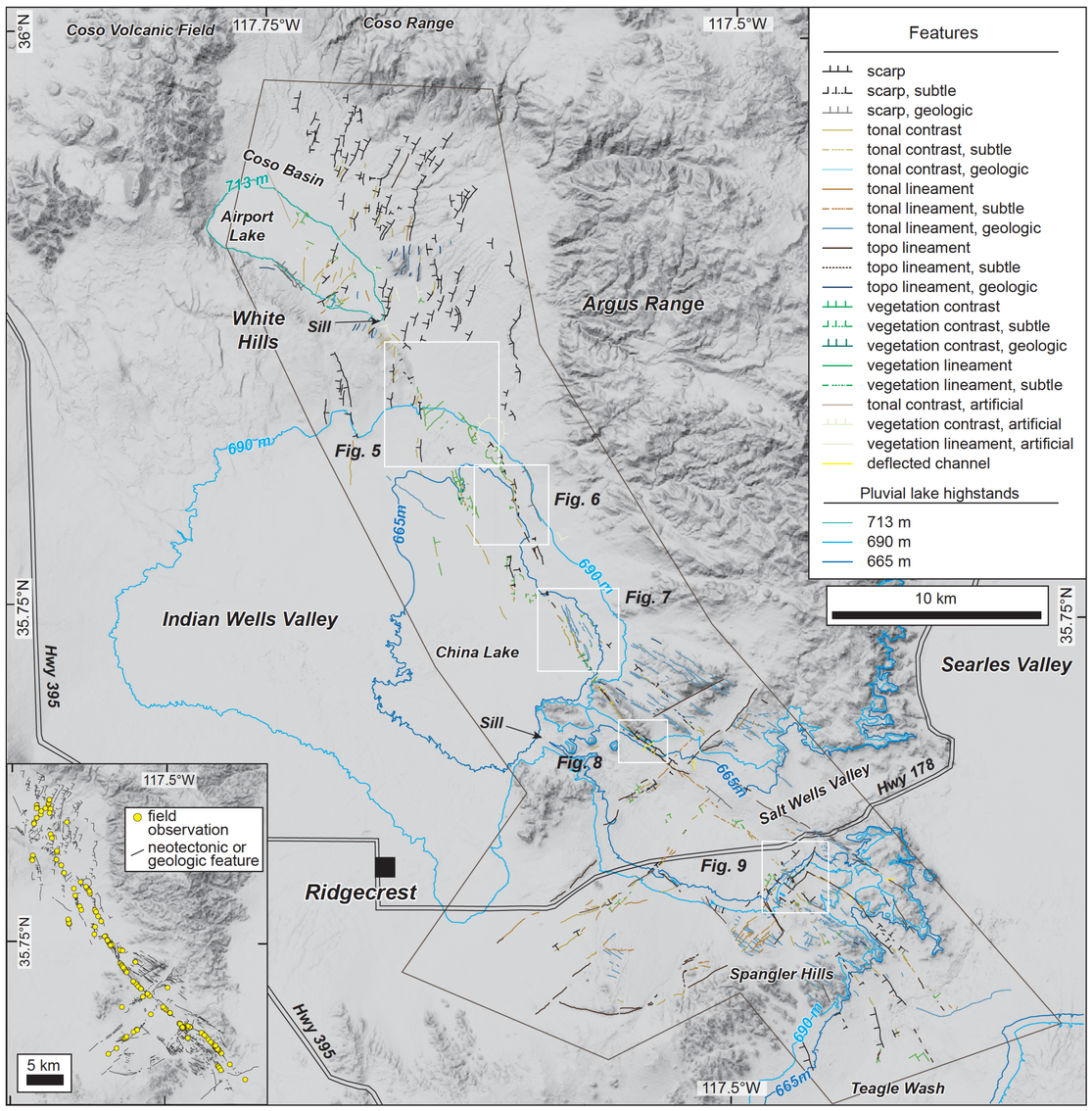

Figure 4. Map of neotectonic and other notable features in the vicinity of the 2019 earthquake ruptures. Brown polygon outlines mapped area. Inset shows distribution of field observations. Pluvial lake highstand elevations in China and Searles Lake Basins are from Rosenthal et al. (2017).

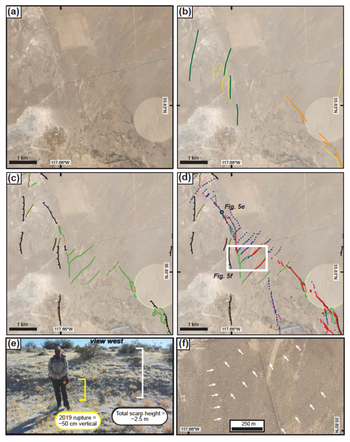

Figure 5. Vegetation lineaments and contrasts at the northern end of the China Lake Basin. (a) Pre-event imagery, (b) previously mapped faults; (c) mapped scarps and vegetation lineaments and contrasts; (d) 2019 surface rupture traces superimposed on mapped features. (e) Field photo of the 2019 rupture that occurred on a pre-existing scarp. (f) Imagery detail illustrating vegetation lineaments.

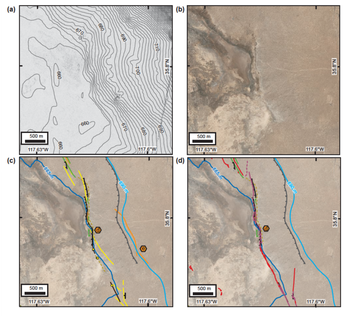

Figure 6. Neotectonic features in the northern China Lake Playa area. (a) Uninterpreted slopeshade of the pre-event 2-m DEM and (b) pre-event imagery. (c) Interpreted neotectonic and other geologic features, previously mapped faults, and late Pleistocene pluvial lake highstands. (d) 2019 M7.1 rupture traces with mapped neotectonic and geologic features.

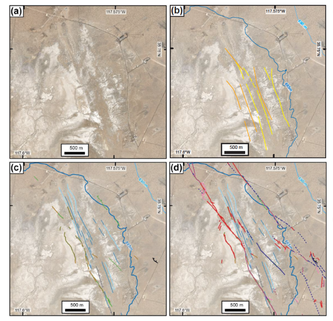

Figure 7: Neotectonic features in the southern China Lake Playa area. (a) Uninterpreted imagery; (b) previously mapped faults; (c) interpreted neotectonic and other geologic features; and (d) 2019 M7.1 rupture traces with mapped neotectonic and geologic features.

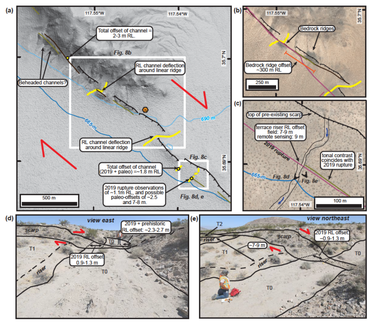

Figure 8: Examples of dextrally offset features and other neotectonic observations from the northern end of Salt Wells Valley. (a) Hillshade of 2-m DEM with neotectonic features and late Pleistocene shorelines. Yellow dots represent locations of field observations. (b) Imagery illustrating ~300 m of dextral offset of a bedrock ridge. (c) Imagery illustrating dextral offset of channel. (d) and (e) field photos illustrating dextral offsets of a channel observed in the 2019 rupture, and larger dextral offsets of terrace risers from older events.

Examples illustrate a variety of fault expression, areas where geologic fabrics obscured active structures, and the successes and failures of previous mapping.

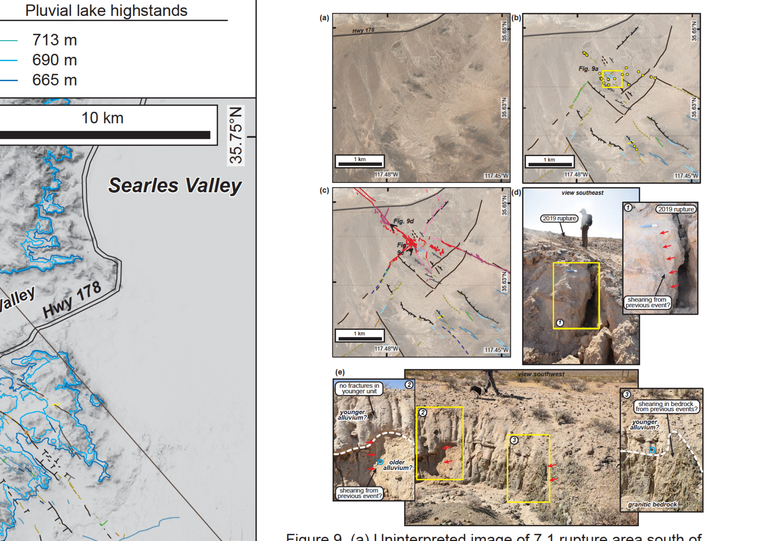

Figure 9. (a) Uninterpreted image of 7.1 rupture area south of Highway 178. No active faults were previously mapped in this area. (b) Neotectonic and other features and (c) 2019 surface rupture traces overlaid on the same image. (d) Field photo illustrating previous vertical shearing in a channel wall, with the 2019 rupture ~10 cm to the right. (e) Field photo showing offset and sheared older alluvium and bedrock on a cross fault subparallel to the M6.4 rupture. Note lens cap for scale.

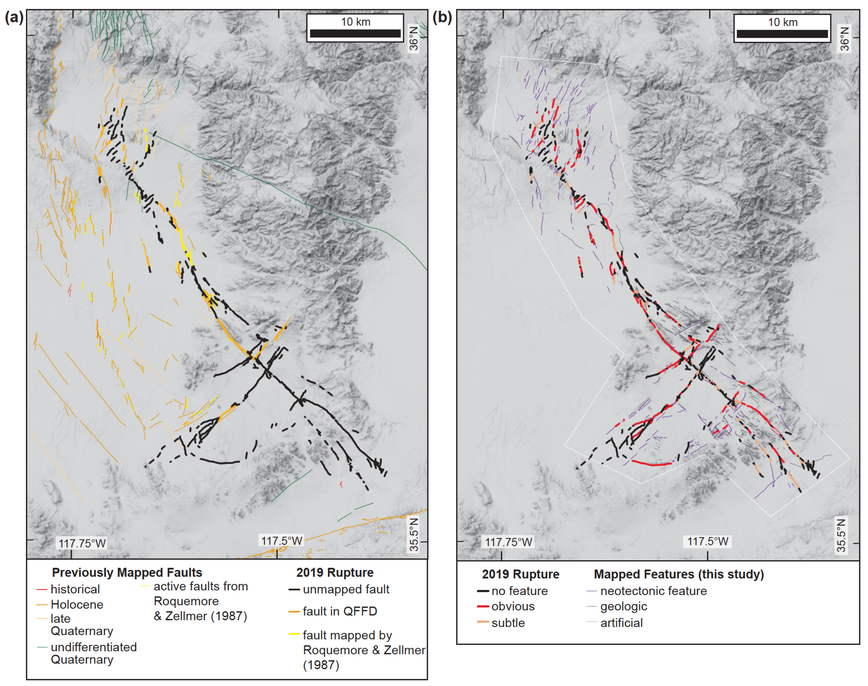

Figure 10. (a) Comparison of the 2019 rupture to faults previously mapped in the QFFD and by Roquemore and Zellmer, 1987. (b) Comparison of the 2019 rupture to the neotectonic features mapped in this study.

- M 7.1: ~34% (18.5/55 km) in QFFD
  additional ~4.3 km (8%) mapped by R&Z
- M 6.4: ~37% (7.7/21 km) in QFFD
- Parts of a few secondary ruptures in QFFD
- M 7.1: ~70% pre-existing; ~45% obvious
- M 6.4: ~59% pre-existing; ~53% obvious
- Most secondary traces also pre-existing

About 50% of the 2019 ruptures could have been recognized as active faults based on obvious features alone, and some additional subtle features might have been recognized based on position between or along strike from more prominent features. Active faults might also have been correctly inferred even in areas with no features, connecting more well-expressed sections.

Results & Conclusions

- Evidence of previous late Quaternary activity is distributed along most of the 2019 surface ruptures and along additional subparallel faults that did not rupture in 2019. These define a distributed network of orthogonal faults.
- Neotectonic features are more prominent outside pluvial lake basins and/or where vertical deformation is more significant.
- In many areas, both the NE- and NW-striking faults appear to follow (and are likely reactivating) an older regional bedrock fabric. This fabric hampers recognition of active faults.
- 50–70% of the 2019 rupture traces could have been recognized as active faults if our analysis had been done before the 2019 events. Thus, the 2019 events would have been less surprising with appropriately systematic neotectonic mapping.
- Areas of distributed faulting such as this region are best represented by a fault zone polygon within which rupture is permitted anywhere, rather than a simplified single proxy fault.

References & Acknowledgements

Kozaci, O., et al. (2019). Rapid post-earthquake reconnaissance and paleoseismic trenching preliminary results for the M6.4 and M7.1 Ridgecrest Earthquake Sequence, Southern California. AGU Fall Meeting 2019 Abstract S31F-0454.

Ponti, D., et al. (2020). Documentation of surface fault rupture and ground-deformation features produced by the 4 and 5 July 2019 Mw 6.4 and Mw 7.1 Ridgecrest earthquake sequence. *Seismol. Res. Lett.* 91(4).

Roquemore, G. R., and J. T. Zellmer (1987). Naval Weapons Center Active Fault Map Series (No. NWC-TP-6828). Naval Weapons Center, China Lake, CA.

Roquemore, G. R. (1981). Active Faults and Associated Tectonic Stress in the Coso Range, California (No. NWC-TP-6270). Naval Weapons Center, China Lake, CA.

Rosenthal, J., et al. (2017). Paleohydrology of China Lake basin and the context of early human occupation in the northwestern Mojave Desert, USA. *Quat. Sci. Rev.* 167, 112-139. 10.1016/j.quascirev.2017.04.023.

U.S. Geological Survey and California Geological Survey (2019). Quaternary fault and fold database for the United States, last accessed Jan 2020, from USGS web site: https://earthquake.usgs.gov/hazards/qfaults/.

Willis, M. J., et al. CalDEM: Ridgecrest, CA Region 2m Digital Surface Elevation Model. Funding by NSF and USGS. Data collection by DigitalGlobe. Distributed by OpenTopography. https://doi.org/10.5069/G998854C.

We thank the Naval Air Weapons Station China Lake for technical assistance and providing access. Valuable discussions with Ralph Klinger, Joanna Redwine, Julia Howe, Sylvia Nicovich, Glenda Besana-Ostman, Kirstyn Cataldo, Marith Reheis, and Lucille Piety greatly improved the field observations along the southern part of the M7.1 rupture. This work was partially funded by the Bureau of Reclamation Dam Safety Office. This study was published in BSSA in August 2020.